© creative

Scientific paper

Synthesis, Characterization and Biological Evaluation of Substituted Pyridine Based Benzo-thiazol Derivatives: In Silico Calculations and ADME Prediction

Iram Akbar,¹ Amir Karim,² Muhammad Iqbal,^{1,*} Rahime Eshaghi Malekshah,^{2,3} Najeeb Ullah,² Yu-Ting Chu,² Saqib Ali,^{4,*} Sodio C. N. Hsu,^{2,5,*} and Muhammad Nawaz Tahir⁶

¹ Department of Chemistry Bacha Khan University Charsadda 24420, KPK, Pakistan.

² Department of Medicinal and Applied Chemistry, Kaohsiung Medical University, Kaohsiung 80708, Taiwan.

³ Department of Chemistry, Semnan University, Semnan, Iran.

⁴ Department of Chemistry, Quaid I Azam University, Islamabad, Pakistan.

⁵ Department of Medical Research, Kaohsiung Medical University Hospital, Kaohsiung 80708, Taiwan.

⁶ Department of Physics, University of Sargodha, Sargodha, Pakistan

* Corresponding author: E-mail: iqbal@bkuc.edu.pk, iqbalmo@yahoo.com Fax: +92-91-6540060

Received: 02-18-2025

Abstract

In this study, a series of new condensation products L_1-L_5 have been synthesized from substituted pyridinecarbaldehydes and 2-aminobenzothiazole and characterized by FTIR, UV-Visible, 1H NMR spectroscopy and ESI-MS analysis. Additionally, compound L_1 was structurally characterized through single-crystal X-ray diffraction study exhibiting four crystallographically independent molecules in the asymmetric unit. All the synthesized compounds exhibited antibacterial activity against Gram-negative and Gram-positive bacteria as well as against *Candida albicans* ATCC 60193 and *Candida tropicalis* ATCC 13803. All the compounds were optimized by using DFT-D method. Total energy values for compounds were calculated then, the reactivity descriptors were theoretically proven by computing the HOMO and LUMO energies. The prediction of ADME properties indicated that all of the compounds exhibit good drug-likeness and pharmacokinetic properties.

Keywords: (E)-N-((6-methoxypyridin-3-yl)methylene)benzo[d]thiazol-2-amine; Crystal structure; Bioactivities; Computational Studies; Swiss ADME.

1. Introduction

2-Aminobenzothiazole (2-ABT) has a significant role in the synthesis of organic compounds due to the presence of the electrophilic amino group (-NH₂) which can yield fused heterocycles.¹ It is an important compound due to its high reactivity, and can be modified according to the needs by the substitution on the benzene ring, making such derivatives ideal for medicinal chemistry.² Riluzole is 2-ABT derivative which has been extensively investigated for its role as a central muscle relaxant and glutamate neurotransmission inhibitor since the 1950s.³ Its derivatives

showed to be promising anticancer candidates, emphasizing targeted delivery systems to enhance efficacy and reduce side effects.⁴ 2-Aminobenzothiazole derivatives have been extensively explored for antimicrobial, anticonvulsant, anti-HIV, analgesic, anti-viral, anti-inflammatory, antileishmanial, antitubercular and anticancer activities. The unique structural features of benzothiazole make them versatile scaffolds for drug development.^{5–15} The presence of electronegative substitution such as halogen (–X) on aromatic ring has shown potent antimicrobial and anti-tuberculosis activities.¹⁶ Another study demonstrated that these compounds have significant role in antifungal

and antibacterial activities against Candida albicans, Aspergillus niger, Staphylococcus. aureus, Streptococci, Escherichia coli, and Pseudomonas.¹⁷

Schiff base is usually obtained by treating amines with an aldehyde or ketone, making an imine or azomethine functionality. 18 This imine (-C=N-) group in Schiff bases is crucial for their impressive biological activities, including anti-bacterial, antifungal, anti-viral, anti-oxidant, anti-leishmanial, anti-convulsant, anti-tumor, analgesic, anti-inflammatory, anti-glutamate, anti-tuberculosis, anti-diabetic, anti-malarial, anthelmintic and herbicidal properties. 19-22 2-Aminobenzothiazol derivatives serve as ideal precursors for the synthesis of Schiff base ligands. The aromatic moiety significantly enhances DNA binding capacity through effective stacking interactions, contributing to the stabilization of the DNA double helix.²³ Schiff bases derived from 2-ABT are suitable for the synthesis of metal complexes as well. These compounds can also be used as catalysts in various industrial applications, including polymerization and fine chemical synthesis.²⁴ Schiff bases of 2-ABT have shown potential ability as chemo-sensors for detecting Hg2+ ions, indicating interesting applications in medicinal and environmental fields. 16 Upadhyay et al. synthesized three novel Schiff bases using 4,6-difluoro-2-aminobenzothiazole. One of those compounds N-((1H-indol-3-yl)methylene)-4,6-difluorobenzothiazole-2-amine demonstrated excellent antimicrobial activity, particularly against fungal strains. 25 Moustafa et al. synthesized a series of compounds derived from 2-ABT showing significant antitumor activity against HeLa cells and COS-7 cells suggesting their potential as new antitumor agents.²⁶

To develop medicinal drugs with minimum side effects, computational studies such as molecular docking, density functional theory (DFT) and absorption, distribution, metabolism, elimination and toxicity (ADMET) are used extensively. These theoretical methods help in prediction of the geometry, interaction with specific target enzyme and possible pharmacokinetic, pharmacodynamics and physicochemical significance.^{27–29}

Inspired by excellent biological potential of 2-aminobenzothiazole compounds, we have synthesized five new Schiff bases using substituted pyridine carboxaldehydes. All compounds were characterized using different analytical techniques including single crystal XRD, ¹H NMR, ESI-MS, FTIR and UV-Visible spectrophotometry. All the compounds were tested for antibacterial, antioxidant and anti-fungal activities experimentally. Furthermore, DFT-D, molecular docking and drug-likeness studies were applied in predicting possible biological activities.

2. Experimental

2. 1. Reagents and Materials

All the chemicals utilized in this study were obtained from Fluka (Switzerland) and all solvents were purchased from Merck (Germany). Both, chemicals and solvents in current study were used without further purification. Distilled water was employed throughout the experiments. Thin layer chromatography was performed using Silica Gel G (Merck Index) pre-coated plates and the spots were visualized by exposure to UV light.

2. 2. Instrumentations

The melting points of the prepared compounds were checked by capillary tube using a Gallenkamp, serial number C040281, UK, an electro thermal M.P. apparatus. FT-IR spectra of the compounds were obtained on Perkin 1,600,300 Laintrisant S.No 95,120 UK from 4000 to 400 cm⁻¹. The UV-Visible spectrophotometer Shimadzu Mod. UV 1800-240 V with 1.0 cm quartz cells was used for spectral analysis. Bruker Avance Digital 300 MHz NMR spectrometer was used for ¹H NMR study. ESI mass spectra were collected on a Waters ZQ 4000 mass spectrometer using methanol as solvent and are presented in Figures 7S-9S. Suitable crystals of L₁ were obtained by slow evaporation of toluene solution. Single crystal X-ray diffraction data was collected on XtaLAB Pro II AFC12 (RINC): Kappa single diffractometer using Mo K α Radiation (λ = 0.71073). The crystal was kept at a temperature of 100 K (± 2 K) and the data was collected by PLATON.³⁰ The structure was solved by direct methods and was refined on F² by the full-matrix least-squares method using the SHELXL-2019 program.³¹

2. 3. Syntheses of Compounds L_1 – L_5

All the compounds L_1 – L_5 were synthesized based on the following method as presented in Scheme 1.

2. 3. 1. Synthesis of L_1

Compound L_1 was synthesized by refluxing an equimolar solution of 6-methoxy-3-pyridinecarboxaldehyde (0.275 g, 2 mmol) with 2-aminobenzothiazole (0.300 g, 2 mmol) in dry toluene for 3 h. The reaction progress was continuously monitored by TLC. After 3 h the reaction mixture was filtered, concentrated to 10 mL and kept for crystallization at room temperature. Yellow crystals appeared in 3 days. Crystals were filtered off and washed with diethyl ether and characterized by single crystal XRD, ¹H NMR, ESI-MS, FTIR and UV-Vis spectrophotometry. Yellow color; m.p. 170 °C; yield: 0.413 g (77%). UV-Vis: $(1.57 \cdot 10^{-3} \text{ M}, \text{ MeOH}) \lambda_{\text{max}} = 263, 294, 350 \text{ nm}.$ Selected FT-IR data (solid): $v_{\text{max}}/\text{cm}^{-1}$ 3061(w), 2981(w), 2949(w), 2852(w), 1690(m), 1600(s), 1560(m), 1492(s), 1473(w), 1452(m), 1427(m), 1346(s), 1311(s), 1284(s), 1257(m), 1219(w), 1154(m), 1102(m), 1059(w), 1010(s), 861(w), 840(s), 818(w), 759(s), 723(s), 664(s), 628(w), 612(m), 527(m). 1 H NMR (300 MHz, CDCl₃): δ 8.83 (s, 1H), 8.19-8.15 (m, 1H), 7.87-7.84 (m, 1H), 7.48 (dd, J =

7.0, 1.8 Hz, 1H), 7.38 (dd, J = 7.2, 1.6 Hz, 1H), 7.35 (s, 1H), 7.33 (d, J = 5.5 Hz, 1H), 7.34–7.29 (m, 1H), 6.79 (d, J = 8.7 Hz, 1H), 3.97 (s, 3H). ESI-MS: m/z calculated for [L₁ = C₁₄H₁₁N₃OS]⁺: 269.06, found: [L₁ + H⁺ = 270.02]⁺.

2 mmol). The final product was characterized by ¹H NMR, FTIR and UV-Vis spectrophotometry. Yellow color; m.p. 133 °C; yield: 0.427 g (79%). UV-Vis (1.57 · 10⁻³ M, MeOH) $\lambda_{\text{max}} = 263$, 294, 350 nm. Selected FT-IR data (solid):

Scheme 1. Synthetic rout followed for compounds L₁-L₅.

2. 3. 1. Synthesis of L₂

For L₂, the same procedure was followed as for L₁ but using 6-methoxy-2-pyridinecarboxaldehyde (0.275 g, 2 mmol). The final product was characterized by 1 H NMR, FTIR and UV-Vis spectrophotometry. Yellow color; m.p. 130 °C; yield: 0.392 g (73%). UV-Vis: $(1.57 \cdot 10^{-3} \text{ M}, \text{MeOH}) \lambda_{\text{max}} = 263, 294, 350 \text{ nm}.$ Selected FT-IR data (solid) $\nu_{\text{max}}/\text{cm}^{-1}$ 3075(w), 3048(w), 3001(w), 2861(m), 1702(s), 1675(w), 1573(m), 1552(m), 1465(m), 1382(w), 1367(m), 1292(m), 1260(w), 1206(s), 1122(w), 1107(s), 1012(s), 985(w), 934(w), 847(s), 827(s), 725(m), 707(s), 626(s), 543(s), 480(s), 414(s). 1 H NMR (300 MHz, CDCl₃): δ 9.05 (s, 1H), 8.62 (s, 1H), 8.37 (d, J = 6.0 Hz, 1H), 8.35 (d, J = 6.0 Hz, 1H), 7.97 (d, J = 6.0 Hz, 1H), 7.84 (d, J = 3.0 Hz, 1H), 7.50–7.35 (m, 1H), 7.88 (t, J = 6.0 Hz, 1H), 4.02 (s, 3H).

2. 3. 1. Synthesis of L₃

For L_3 , the same procedure was followed as for L_1 but using 3-methoxy-2-pyridinecarboxaldehyde (0.275 g,

 $v_{\text{max}}/\text{cm}^{-1}$ 3393(w), 3270(w), 3056(w), 2913(w), 2726(w), 1629(m), 1525(m), 1440(m), 1368(w), 1105 (m), 1068(w), 1018(w), 962(w), 917(m), 886(m), 841(w), 737(s), 715(s), 681(m), 628(w), 429(s). ^{1}H NMR (300 MHz, CDCl₃): δ 9.03 (s, 1H), 8.61 (s, 1H), 8.35 (d, J = 6.0 Hz, 1H), 7.95 (d, J = 6.0 Hz, 1H), 7.82 (d, J = 6.0 Hz, 1H), 7.46 (d, J = 3.0 Hz, 1H), 7.40–7.33 (m, 1H), 6.87 (t, J = 6.0 Hz, 1H), 4.02 (s, 3H).

2. 3. 1. Synthesis of L₄

For L₄, the same procedure was followed as for L₁ but using 5-chloro-2-pyridinecarboxaldehyde (0.283 g, 2 mmol). The final product was characterized by 1 H NMR, ESI-MS, FTIR and UV-Vis spectrophotometry. Yellow color; m.p.134 °C; yield: 0.445 g (81%). UV-Vis (1.57 · 10⁻³ M, MeOH) $\lambda_{\rm max} = 263$, 294, 350 nm. Selected FT-IR data (solid): $\nu_{\rm max}/{\rm cm}^{-1}$ 3390(w), 3273(w), 3059(w), 2912(w), 2725(w), 1916(w), 1632(s), 1526(s), 1444(s), 1365(w), 1105(s), 1064(w), 1016(m), 961(w), 914(m), 886(m), 842(m), 739(s), 719(s), 685(m), 431(s). 1 H NMR (300 MHz, CDCl₃): δ 10.16 (s, 1H), 8.43–8.39 (m, 2H), 8.39 (s, 1H), 8.10 (d, J = 2.0 Hz, 2H), 8.09–8.05 (m, 2H), ESI-MS:

m/z calculated for $[L_4 = C_{13}H_8ClN_3S]^+$: 273.01, found: $[L_4 + H^+ = 273.93]^+$.

2. 3. 1. Synthesis of L₅

For L₅, the same procedure was followed as for L₁ but using 5-bromo-2-pyridinecarboxaldehyde (0.372 g, 2 mmol). The final product was characterized by 1 H NMR, ESI-MS, FTIR and UV-Vis spectrophotometry. Yellow color; m.p. 160 °C; yield: 0.482 g (76%). UV-Vis (1.57 · 10^{-3} M, MeOH) $\lambda_{\rm max} = 263$, 294, 350 nm. Selected FT-IR data (solid): $\nu_{\rm max}/{\rm cm}^{-1}$ 3390(w), 3270(w), 3053(w), 3026(w), 2918(w), 2731(w), 1921(w), 1622(m), 1499(w), 1439(w), 1107(s), 1065(w), 1012(w), 966(w), 920(m), 885(m), 849(m), 740(s), 715(s), 486(m), 429(s). 1 H NMR (300 MHz, CDCl₃): δ 10.18 (s, 1H), 8.43 (d, J = 1.7 Hz, 2H), 8.40 (s, 1H), 8.12–8.09 (m, 2H), 8.08 (s, 2H), ESI-MS: m/z calculated for [L₅ = $C_{13}H_8{\rm BrN}_3{\rm S}]^+$: 316.90, found: [L₅ + H⁺ = 317.83]⁺.

2. 4. Biological Studies

2. 4. 1. Antibacterial Activity

The *in vitro* antibacterial evaluation of the synthesized compounds L_1 – L_5 was performed against five types of pathogens: three Gram-negative bacteria (*Escherichia coli, Klebsiella pneumoniae* and *Pseudomonas aeruginosa*) and two Gram.positive bacteria (*Staphylococcus aureus* and *Streptococcus pyogenes*). The antibacterial assay was conducted at pH 7.4 \pm 0.2, with a final inoculum concentration of 10^5 cfu/mL. The test solutions were prepared for all compounds in dimethyl sulfoxide (DMSO) at concentrations of 2, 10, 20, 40, 60, 80 and $100~\mu$ g/mL and diluted in Mueller–Hinton broth. Then the solutions were incubated at 37 °C and evaluated after 24 h against bacteria.

2. 4. 2. Antioxidant Activity

All the compounds were tested for free radical scavenging ability using 1,1-diphenyl-2-picryl-hydrazyl free radical (DPPH) as standard. The absorbance of the samples was estimated at 515 nm on a UV-Visible spectrophotometer as compared to a blank of ethanol. Three different concentrations 50, 100 and 200 μ g mL⁻¹ were prepared and stored in the dark. A 500 μ L solution of DPPH added to 250 μ L of each test samples of L_1 – L_5 . Then all compounds containing DPPH were incubated for 30 min at room temperature. The experiments were performed in triplicate and percentage of inhibition based on the DPPH scavenging ability was calculated using the following formula (1):

DPPH scavenging effect
$$\% = \frac{A_0 - A_s}{A_0}$$
 (1)

where A_o , is the absorbance of the control sample (DPPH solution) and A_s is the absorbance of the sample along with DPPH solution after incubating for 30 min.

2. 4. 3. Anti-fungal Activity

All the ligands were examined for antifungal activity using fungal colony of *Candida albicans* ATCC 60193 and *Candida tropicalis* ATCC 13803 and percent inhibition was calculated using formula (2).

Fungal growth inhibition (%) =
$$\frac{A-B}{A} \times 100$$
 (2)

where *A* is the diameter of the fungal colony in the control plate and *B* is the diameter of the fungal colony after treating with samples.

2. 5. Computational Studies

2. 5. 1. DFT-D Calculations

In current study, all compounds were designed in Material Studio 2017 and the computational calculations were attained using DFT-D in gaseous phase.^{33,34} In order to describe the exchange correlation effects, the generalized gradient approximation (GGA) with the Perdew–Burke–Ernzerhof (PBE) function was applied in the calculations and performed by the Dmol³ software in this package.³³ The resultant optimized structures, HOMO/LUMO distributions, energies and the chemical reactivity descriptors are given in Figures 6 and 7, and Tables 5 and 6, respectively. All optimized compounds were saved in Mol² file format to study molecular docking.

2. 5. 2. Molecular Docking Study

All the compounds were docked with Gram-negative bacteria *E. coli* DNA gyrase B in complex with small molecule inhibitor (PDB code 4DUH) and Gram-positive bacteria *Streptococcus pneumonia* (PDB code 4MOT) which were downloaded from the Protein Data Bank server https://www.rcsb.org/structure/4mot and https://www.rcsb.org/experimental/4duh. Molecular docking calculations were performed using Molegro Virtual Docker (MVD). The dimensions for 4DUH and 4MOT were set $21.24 \cdot 11.84 \cdot 24.16$ and $21.38 \cdot 29.05 \cdot 2.13$, respectively. Additionally, five poses were set in the software. The binding interactions for specific receptor sites with ligands were studied by Biovia Discovery Studio 2016.³⁵

2. 6. ADMET Profiling

In order to understand biological efficacy of compounds presented in this work ADMET study was employed. This method helps in predicting pharmacokinetic and pharmacological studies containing log $P_{\rm o/w}$, bloodbrain barrier (BBB) permeate, gastrointestinal (GI) absorption, total polar surface area (TPSA), bioavailability and Lipinski's rule of the newly synthesized compounds. ADME studies were performed by Swiss ADME using an online platform. After that, the predictive model of Egan's Boiled-egg and the bioavailability radar were calculated to

investigate the central nervous system (CNS) and measure their oral bioavailability for human health.

3. Results and Discussion

3. 1. FTIR Discussion

FTIR spectroscopy is a highly valuable technique for the structural determination of the synthesized compounds. The formation of a Schiff base can be confirmed by the disappearance of characteristic carbonyl (C=O) and amine (-NH₂) peaks and the appearance of distinct azomethine (HC=N-), band in the FTIR spectrum. FTIR spectra of Schiff bases are presented in Figure 1S. The spectra of L₁-L₅ showed medium to strong band in the range of 1622-1690 cm⁻¹ typically corresponding to the stretching vibration of azomethine (HC=N-), while the weak band in the region of 3048-3061 cm⁻¹ corresponded to aromatic (Ar-H).36 The weak absorption bands in the range of 2861-2918 cm⁻¹ typically indicated azomethine C-H group. The presence of strong band in the region of 725-759 cm⁻¹ belongs to (C-S-C) thiazine group.²⁵ The stretching frequency of pyridine group (-C=N-) was observed in the range of 1499-1560 cm⁻¹.37

3. 2. UV-Visible Spectroscopic Study

The UV-Visible spectral study of the synthesized compounds $\mathbf{L}_1\mathbf{-L}_5$ was conducted at room temperature in methanol. All the absorption spectra of $\mathbf{L}_1\mathbf{-L}_5$ were compared to the starting material, 2-aminobenzothiazole as shown in Figure 1. The absorption band at 263 nm is primarily attributed to the $\pi \to \pi^*$ transitions of the pyridine moiety. The small shoulder peak at 294 nm revealed distinctive $\pi \to \pi^*$ transitions reinforcing the presence of aromatic rings which could be particularly ascribed to the π -electrons present in 2-aminobenzothiazole part of the Schiff base as observed in unreacted form as well. The appearance of new absorption band at 350 nm is evidence of $n \to \pi^*$ transitions of azomethine group. 20,36,39

3. 3. ¹H NMR Study

The ¹H NMR spectra of compounds L₁–L₅ were measured in CDCl₃ by using TMS as an internal reference and are presented in Figures 2S–6S. The multiple signals corresponding to aromatic protons were observed in the range of 8.11–6.78 ppm.²⁵ A signal in range 8.6–7.9 ppm corresponded to aromatic protons in the pyridine ring. The peaks in the range of 3.97–4.2 ppm confirm the presence of methoxy substituents in compounds L₁–L₃.⁴⁰ The peaks observed at 8.82 (L₁), 8.83 (L₂), 9.03(L₃), 10.16 (L₄), and 10.18 (L₅) ppm are assigned to azomethine protons which is a strong evidence for the synthesis of the mentioned Schiff bases.^{41,42} The observed shifting of azomethine protons due to the influence of electron-withdraw-

ing and electron-donating substitution on pyridine group of the Schiff bases is in line with the literature. 41,42

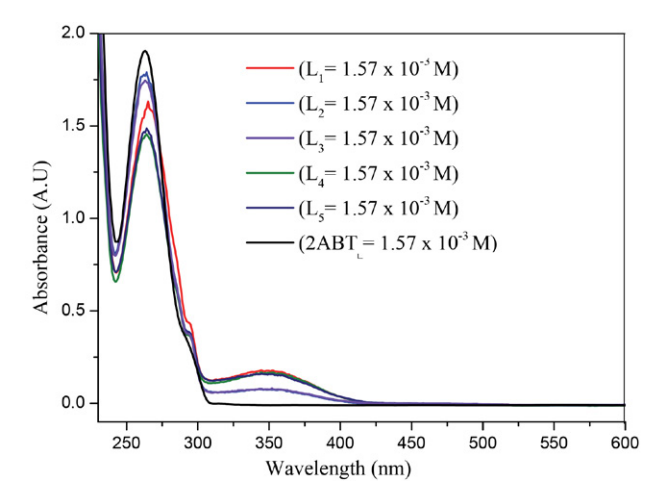


Figure 1. UV-Visible spectra of compounds $L_1\text{-}L_5$ and 2-amin-obenzothizole.

3. 4. Structural Description

Compound L₁ crystalizes in monoclinic crystal system with space group C 2/c while the crystal structure and atomic numbering scheme are illustrated in Figure 2. The unit cell dimensions and crystallographic parameters are summarized in Table 1, while the important bond lengths and bond angles are listed in Table 2. The azomethine (-C=N-) bond length was found to be consistent with values reported in the literature.¹⁶ The torsion angles C₈-C₉- $C_{13} - S_{12} = 179.2(3)^{\circ}$ and $C_7 - N_2 - C_8 - C_9 = -179.7(3)^{\circ}$ show that the configurations about the C=N bonds are anti (1E).⁴³ The specific spatial orientation of the molecules enables O-atom of methoxy group to participate in C-H...O interaction with the adjacent molecule of the lattice. This interaction of molecules is shown in Figure 3. Since there are no O/N/F-H···O/N/F functionalities in the molecule, there is no H-bonding in the crystal lattice and the packing diagram is shown in Figure 4.

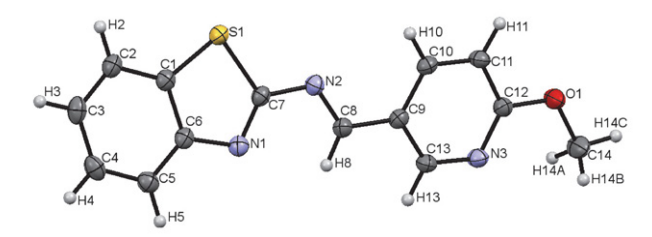


Figure 2. Structure and atom numbering scheme of L₁.

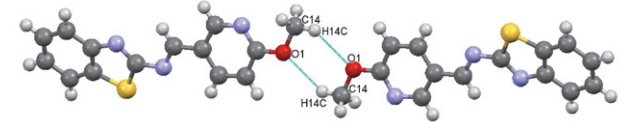


Figure 3. C–H···O interactions (shown blue) exhibited by molecules in lattice.

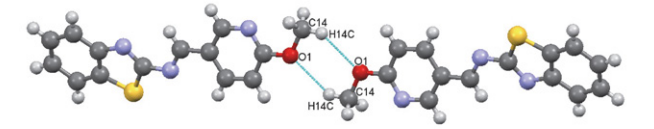


Figure 4. Packing diagram of molecules of L_1 as viewed along b-axis.

Table 1. Crystal data and structure refinement for compound L1.

Empirical formula	$C_{14}H_{11}N_3O_S$
Formula weight	269.32
Crystal system	monoclinic
Space group	C 2/c
a/Å, b/Å, c/Å	47.9676(16), 4.5345(3), 11.3392(7)
α/°, β/°, γ/°	90, 92.390(5), 90
Volume/Å ³	2464.2(2)
Z	8
$\rho_{\rm calc}{\rm g/cm^3}$	1.452
μ/mm^{-1}	0.257
F(000)	1120
Goodness-of-fit on F^2	1.051
Reflections collected	2416
Independent reflections	2166 [$R_{\text{int}} = 0.1242$,]
Data/restraints/parameters	2416/0/173

3. 5. Antibacterial Assay

All the synthesized compounds $\mathbf{L_1}$ – $\mathbf{L_5}$ prevented growth of the microorganisms (Gram-negative and Gram-positive bacteria) as shown by the data given in Table 3. All the compounds were found to be good antibacterial agents against five different types of bacteria. The minimum inhibitory concentrations (MICs, μ g/mL) of compounds $\mathbf{L_1}$ – $\mathbf{L_3}$ demonstrated excellent antibacterial activity compared to compounds $\mathbf{L_4}$ and $\mathbf{L_5}$. All compounds were compared to the standard antibiotic ciprofloxacin. In addition, MIC of compound $\mathbf{L_1}$ was lower than inhibitory concentration of ciprofloxacin and other compounds against *E. coli*, *P. aeruginosa* (–), *S. aureus* (+) and *S. pyogenes* (+). The results demonstrated that com-

pounds L_1 – L_5 showed good activity against Gram-negative compared to Gram-positive bacterial stains. The experimental data were found to be in good agreement with the theoretical results (quantum molecular descriptors and molecular docking). Also, these compounds can obstruct and destroy respiration process of the studied organisms due to the presence of heterocyclic rings containing S and N atoms. ^{44,45} Lipophilicity is a significant factor to control antimicrobial activity. Compounds L_1 – L_5 showed high lipophilicity, which may subsequently promote penetration through the lipid layer of the cell membrane. ⁴⁶ Additionally, lipophilicity and delocalization of π -electrons in the structure of a bioactive molecule have been found to play parallel roles in the enhancement of cell death. ⁴⁷

3. 6. Antioxidant Studies

Reactive oxygen and nitrogen species (RONS) as free radicals that can induce severe oxidative damage on biomacromolecules like DNA, lipids and proteins. Hence, recent investigations have focused on synthesizing novel heterocyclic compounds as potent antioxidants due to their pharmaceutical significance.⁴⁸ In this study, compounds with methoxy substituent (L_1-L_3) exhibited slightly higher activity than the compounds containing halogen groups as shown in Figure 5. Furthermore, L₁ having OMe group on para position with respect to the azomethine functionality revealed good antioxidant activity as compared with other compounds L_2 , L_3 and other halogen-substituted compounds. Halo groups destabilize the free radicals while methoxy groups stabilize the radicals to some extent which might be attributed to the high electronic density. Furthermore, increase in concentration of the compounds resulted in a decrease in the DPPH radical scavenging ability, indicating that the oxidants at low concentrations were most effective.49

3. 7. Anti-fungal Activity

The anti-fungal screening data revealed that all the compounds L_1 – L_5 were active against C. albicans ATCC

Table 2. Selected bond lengths, bond angles, and torsion angles for compound $L_{\rm 1}$

Bond le	engths (Å)	Bond ang	les (°)	Torsion angles (°)
C_1-S_1	1.7302(18)	$C_2 - C_1 - N_1$	115.07	$C_8 - N_2 - C_7 - S_1$ 166.6 (2)
$C_7 - N_1$	1.301(2)	$C_2 - N_1 - C_7$	110.52	$C_8 - N_2 - C_7 - N_1 - 13.7 (5)$
S_1-C_7	1.7511(16)	$C_2 - S_1 - C_7$	88.910	$C_8 - C_9 - C_{13} - S_{12}$ 179.2 (3)
$C_7 - N_2$	1.391(2)	$N_1 - C_7 - S_1$	116.30	$C_7 - S_1 - C_2 - C_1 \qquad -0.2 (2)$
N_1-C_7	1.301(2)	$S_1 - C_7 - N_2$	115.41	$C_7 - S_1 - C_2 - C_3$ 180.0 (3)
N_2-C_8	1.284(2)	$N_1 - C_7 - N_2$	128.23	$C_7 - N_1 - C_1 - C_6$ 179.8 (3)
$N_3 - C_{12}$	1.324(2)	$C_7 - N_2 - C_8$	118.26	$C_7 - N_1 - C_1 - C_2 - 0.3 (4)$
$C_{13}-N_3$	1.343(2)	$C_{10}-N_3-C_{11}$	116.09	$C_7 - N_2 - C_8 - C_9 - 179.7$ (3)
$C_{12}-O_1$	1.349(2)	$N_3 - C_{11} - O_1$	119.55	
$O_1 - C_{14}$	1.4403(19)	$C_{11}-O_1-C_{14}$	117.01	

60193 and *C. tropicalis* ATCC 13803 with diameter of inhibition area ranging from 20–26 and 32–34 mm, respectively. As can be seen from Table 4, all compounds showed higher antifungal effects compared to the standard drug fluconazole.

3. 8. DFT-D Calculations

Optimization based on DFT-D was performed to obtain the most stable structures for all compounds as shown in Figure 6. Total energies for compounds L_1-L_5 were calculated to be -1169.372, -1169.372, -1171.135, -1514.971, and -1068.565 kcal/mol, respectively as shown in Table 5.

3. 9. HOMO and LUMO Orbitals

The HOMO electron density of compounds L_1 – L_5 is mainly distributed over aromatic groups and imine group while the LUMO electron density distribution extends to N and S atoms as shown in Figure 7.

3. 10. Quantum Molecular Descriptors

Recently, researches are employing DFT calculations to obtain quantum chemical parameters for prediction of biological properties. The quantum chemical descriptors such as the ionization potential (I), electron affinity (A),

Table 3. Minimum inhibitory concentration (MIC) values of the compounds L_1 – L_5 (µg/mL).

Compound	E. coli (-)	K. pneumoniae (-)	P. aeruginosa (–)	S. aureus (+)	S. pyogenes (+)
${L_1}$	7.5 ± 0.11	6.5 ± 0.81	8.4 ± 1.73	8.9 ± 0.21	9.3 ± 0.42
L_2	7.9 ± 0.64	6.9 ± 0.98	8.6 ± 1.73	9.6 ± 0.24	10.8 ± 0.47
L_3	7.0 ± 0.45	6.9 ± 0.25	7.0 ± 0.35	9.3 ± 0.55	10.0 ± 0.43
L_4	9.5 ± 0.01	7.6 ± 0.43	9.3 ± 0.32	9.8 ± 0.89	11 ± 0.12
L_5	9.9 ± 0.82	7.9 ± 0.76	10.9 ± 0.19	9.8 ± 0.72	12 ± 1.12
Ciprofloxacin	9.8 ± 1.28	4.8 ± 0.08	9.8 ± 0.08	9.12 ± 0.85	10.5 ± 0.41

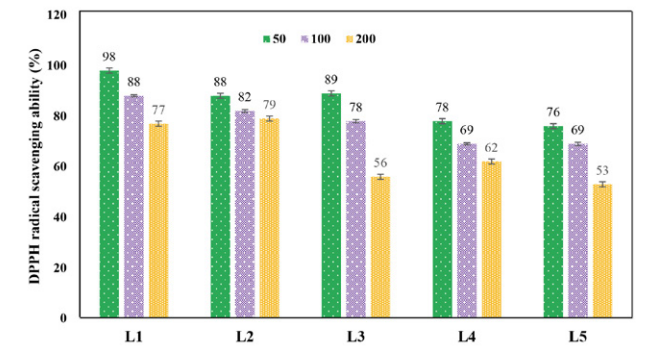


Figure 5. Histogram representation of DPPH free radicals scavenging potentials of the compounds L_1 – L_5 relative to ascorbic acid taken as 100%.

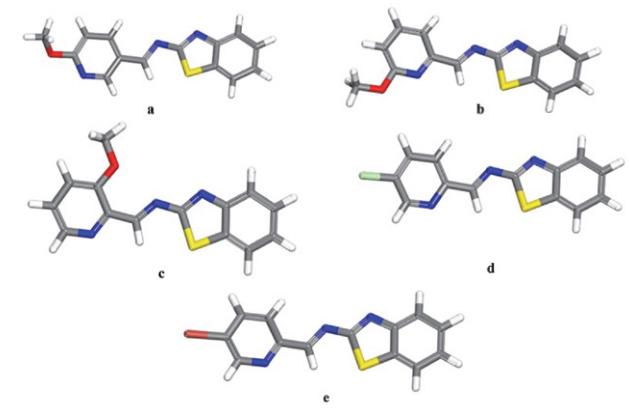


Figure 6. Optimized structures L_1 – L_5 (a–e) based on DFT-D method using DMol³ module in Material Studio 2017.

Table 4. The diameter of antifungal studies of compounds L_1 – L_5 against C. albicans ATCC 60193 and C. tropicalis ATCC 13803

Compounds	L_1	L_2	L_3	L_4	L_5	Fluconazole
C. albicans ATCC 60193	24	23	26	22	20	17
C. tropicalis ATCC 13803	32	32	33	32	34	31

Table 5. The energy parameters resulted from DFT-D method for compounds L1-L5.

com- pounds	Sum of atomic energies	Kinetic	Electrostatic	Exchange- correlation	Spin polarization	DFT-D correction	Total DFT-D energy
$\overline{L_1}$	-1169.372	-30.443	0.278	1.867	-67.441	-0.029	-1239.331
L_2	-1169.372	-30.434	0.272	1.866	-67.441	-0.029	-1239.331
L_3	-1171.135	-10.245	0.155	2.275	1.661	-0.021	-1177.310
$\mathbf{L_4}$	-1514.971	-31.533	0.620	1.639	-78.003	-0.024	-1593.868
L_5	-1068.565	-27.667	0.660	1.625	-61.716	-0.025	-1132.322

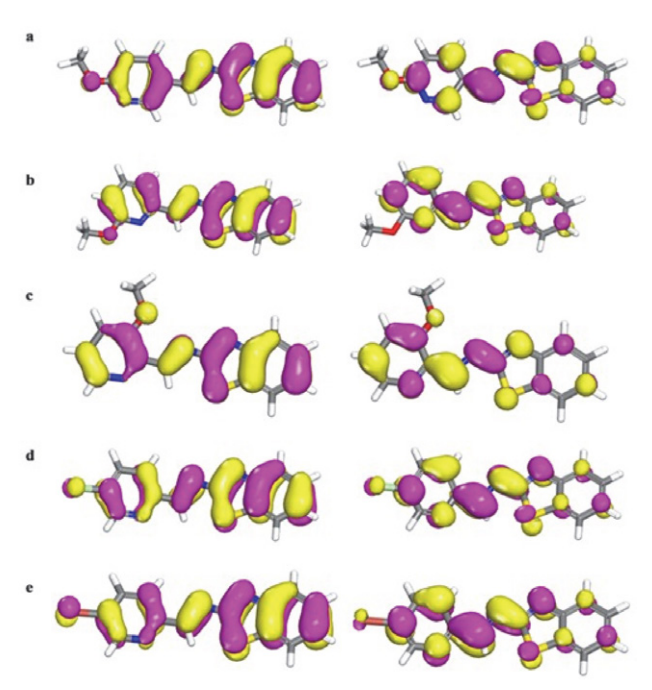


Figure 7. Electron density distributions, HOMO (left) and LUMO (right) orbitals of the compounds L_1 – L_5 (corresponding to a–e, respectively).

3. 11. Molecular Modeling Studies

To understand protein-ligand interactions and drug development affinity of the synthesized compounds toward the targeted proteins, the in silico molecular docking technique using MVD was employed. The molecular docking results and the interactions with receptors are presented in Table 7. The compounds showed good binding orientation in the binding pocket of *E. coli* (PDB code 4DUH) and S. pneumoniae (PDB code 4MOT). Compounds L₁-L₅ with 4DUH revealed a binding affinity of -95.750, -89.837, -98.960, -90.801, and -91.229 kcal/mol. While with 4MOT the lowest possible binding energies for compounds L₁-L₅ were displayed at -107.148, -117.347, -122.728, -103.724, and -104.470 kcal/mol, respectively. Compounds L₁-L₃ revealed the higher binding affinity as compared with L4-L5 in both of receptors in good accord with energy gap (E_{σ}) . 3D and 2D predictions on both of proteins displayed the intermolecular interactions of ligands with amino acid residues in active site from the best docking pose. Docking score of all investigated compounds with S. pneumoniae exhibited negative binding energy, suggesting their high hydrophobic interactions. 2D and 3D views of the non-bonded interactions

Table 6. The calculated quantum chemical parameters obtained from energy gap.

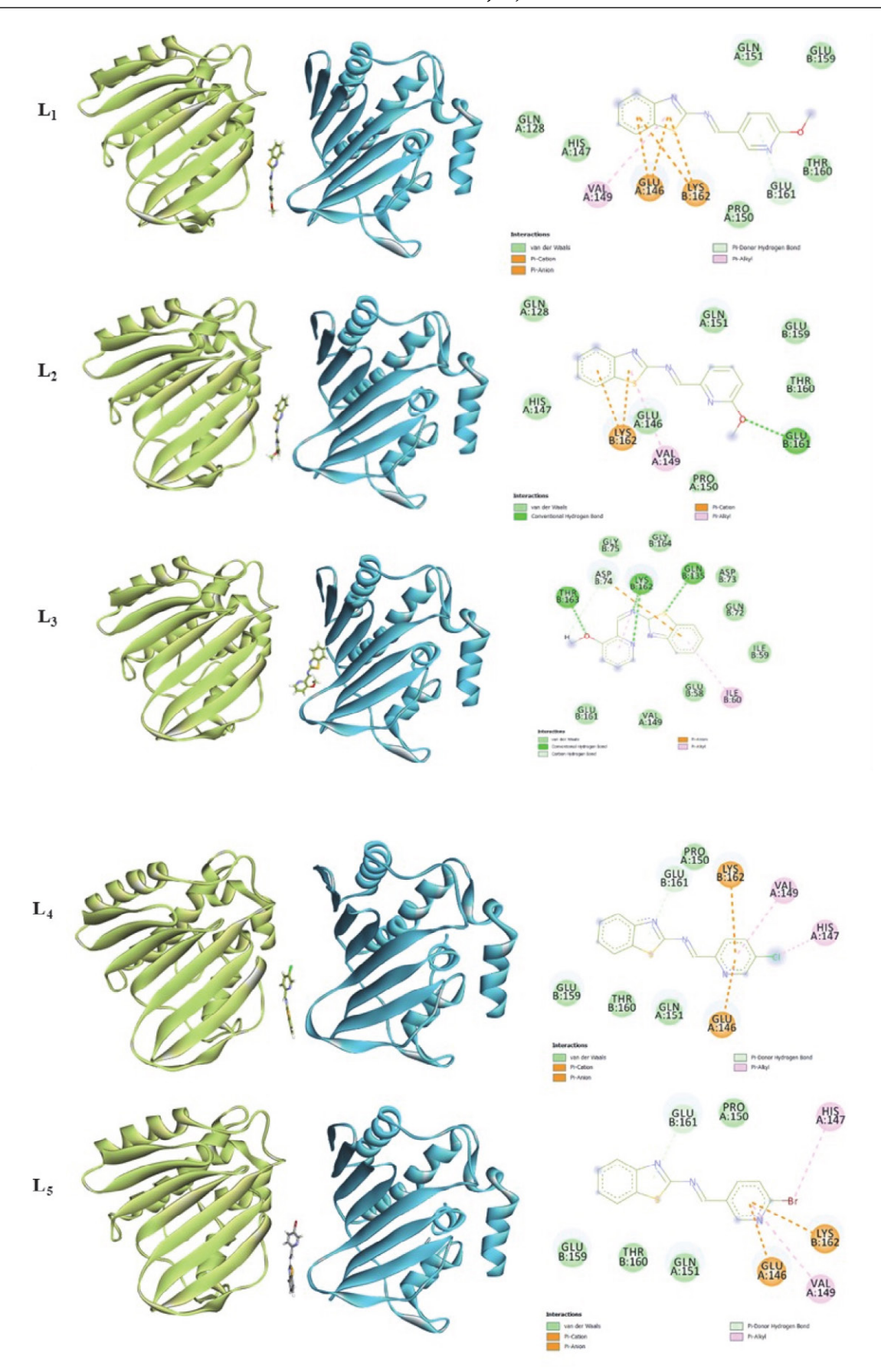
compounds	НОМО	LUMO	$E_{ m g}$	I	A	$\eta = I - A/2$	X	$\mu = -X$	$w = \mu \cdot \mu/2\eta$
${L_1}$	-6.224	-3.727	2.5	6.22	3.73	1.25	4.98	-4.98	9.914
L_2	-6.306	-3.574	2.73	6.31	3.57	1.37	4.94	-4.94	8.93
L_3	-5.768	-3.707	2.06	-5.77	-3.71	1.03	4.74	-4.74	10.889
L_4	-6.435	-3.625	2.81	6.44	3.63	1.41	5.03	-5.03	9.00
L_5	-6.369	-3.636	2.73	6.36	3.5	1.37	4.93	-4.93	8.49

chemical potential (μ), global hardness (η), dipole moment (μ) , and the electrophilicity index (ω) were calculated by HOMO and LUMO energy gaps obtained from the DFT-D results. The higher energy gap ($\Delta E = \text{HOMO} - \text{LUMO}$) imparts less reactivity, less polarizability and more stability to molecule and vice versa. Based on the observed ADME results of energy gaps as listed in Table 6, compound L₃ is less stable and more lipophilic indicating more reactivity. Soft molecules have a lower energy gap than hard molecules and may easily transfer electrons to acceptors, making them more reactive and interacting with biomacromolecules as targets in the biological systems. Consequently, L3 and L1 showed more inhibitory activities. Additionally, L_4 had high chemical hardness (η) as compared to other compounds, leading to the most stable and least reactive compound for the biological activity. Compound L4 exhibited the highest Lewis acid character due to high electronegativity (χ). Global electrophilicity (ω) was found to be significant, indicating that the electrophilic index confirms biocidal property to kill the microbes. 50,51 In addition, L₃ and L₁ can kill cancer cells more than others due to higher value of electrophilicity index (ω).¹⁵

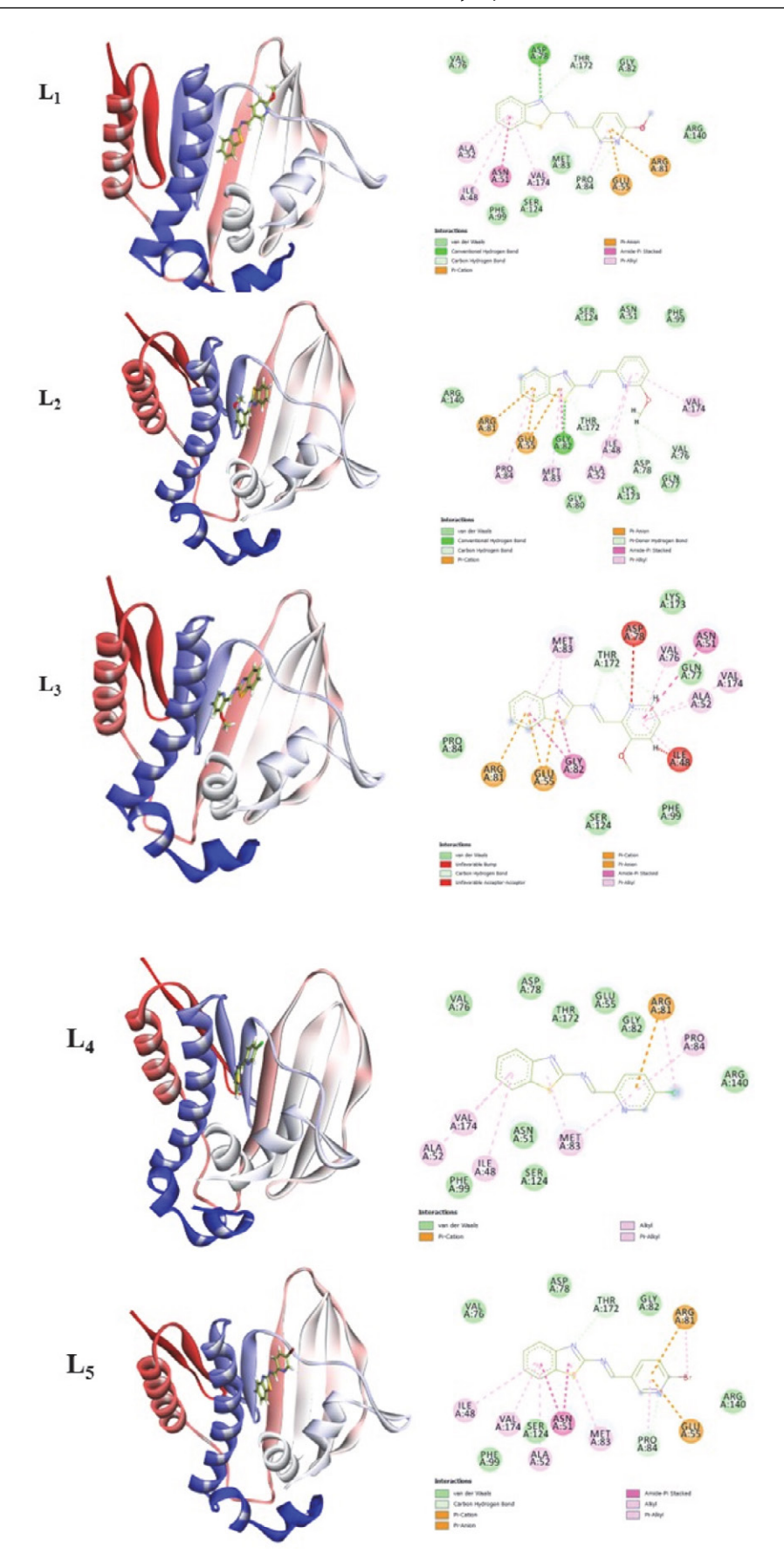
between structures were docked onto *E. coli* (PDB code 4DUH) or *S. pneumoniae* (PDB code 4MOT) and are shown in Figures 8 and 9.

3. 12. Drug Likeness and *In-Silico* Bioactivity Prediction Using Swiss ADME

The behavior of molecules in humans is influenced by the structural features including bioavailability, transport properties, affinity, reactivity, toxicity, and metabolic stability. Table 8 presents the permeability levels of compounds L₁–L₅, describing their potential for molecular transport across the blood–brain barrier (BBB) and intestinal membranes. But these compounds were not cleared from the central nervous system (CNS) by the P-glycoprotein. Moreover, these compounds had high gastrointestinal (GI) absorption, indicating a high absorbance in the human intestine, showing high GI absorption. Furthermore, all of the tested compounds have a bioavailability score of 0.55, showing a moderate level of bioavailability. They obey Lipinski's first rule, signifying that these compounds can be developed as orally active small anti-in-



 $\textbf{Figure 8.} \ 3 \text{D and 2D dimensions of results of intramolecular interactions for compounds } \ \textbf{L}_{1} - \textbf{L}_{5} \ \text{with } \textit{E. coli.}$



 $\textbf{Figure 9.} \ \ \textbf{3D} \ \ \textbf{and 2D} \ \ \textbf{diagrams of intramolecular interactions of compounds} \ \ \textbf{L_1-L_5} \ \ \textbf{with S.} \ \ \textbf{pneumoniae}.$

Akbar et al.: Synthesis, Characterization and Biological Evaluation ...

Table 7. Docking of compounds into E. coli (PDB code 4DUH) and S. pneumoniae (PDB code 4MOT)

compounds	Docking score (kcal/mol)	Interacting residues with 4DUH
$\overline{L_1}$	-95.750	Van der Waals (Pro A:150, Thr B:160, Glu B:159, Gln A:151, His A:147, Gln A:128), π -donor hydrogen bond (Gln B:161), π -alky (Val A:149).
L_2	-89.837	Van der Waals (Gln A:128, His A:147, Gln A:151, Thr B:160, Glu B:159, Glu B:146, Pro A:150), π-alky (Val A:149), hydrogen bond (Glu B:161).
L_3	-98.960	Van der Waals (Gly B:75, Gly B:164, Asp B:73, Gln B:72, Ile B:59, Glu B:58, Val A:149, Glu B:161), hydrogen bond (Thr B:163, Lys B:162, Gln B:135), π-alky (Ile B:60).
L_4	-90.801	Van der Waals (Gln A:151, Thr B:160, Glu B:159, Pro A:150), carbon hydrogen bond (Gln B:161), π -alky (His A:147, Val A:149).
L_5	-89.837	Van der Waals (Glu B:161, Glu B:159, Thr B:160, Glu B:159, Pro A:150, Thr B:151), π -alky (His A:147, Val A:149), hydrogen bond (Glu B:161).
	Docking score (k	cal/mol) Interacting residues with 4MOT
L ₁	-107.148	Van der Waals (Val A:76, Thr A:172, Phe A:99, Ser A:124, Gly A:82, Arg A:84), carbon hydrogen bond (Pro A:84), alkyl and π-alkyl (Ile A:48, Pro A:84, Met A:83, Ala A:52, Val A:174), hydrogen bond (Asp A:78), amid π-stacked (Asn A:51).
L_2	-122.728	Van der Waals (Ser A:124, Phe A:99, Asn A:51, Gln A:77, Lys A:173, Gly A:80), hydrogen bond (Gly A:82), carbon hydrogen bond (Asp A:78, Thr A:172), alkyl and π -alkyl (Pro A:84, Met A:83, Ala A:52, Val A:174, Ile A:48).
L_3	-122.728	Van der Waals (Pro A:84, Lys A:173, Gln A:77, Ser A:124, Phe A:99), amid-π stacked (Asn A:51, Gly A:82), π-alkyl (Met A:83, Val A:174, Ala A:52, Val A:76, Ile A:48), carbon hydrogen bond (Thr A:172).
L_4	-103.724	Van der Waals (Val A:76, Asp A:78, Thr A:172, Glu A:55, Phe A:99, Ser A:124, Gly A:82, Asn A:51), alkyl and π-alkyl (Ile A:48, Pro A:84, Met A:83, Ala A:52, Val A:174).
L ₅	-104.470	Van der Waals (Val A:76, Asp A:78, Glu A:55, Ser A:124, Phe A:99, Gly A:82, Arg A:140), carbon hydrogen bond (Thr A:172), amid π -stacked (Asn A:51), alkyl and π -alkyl (Pro A:84, Met A:83, Ala A:52, Val A:174, Ile A:48).

Table 8: Prediction of the toxicity pharmacokinetic properties based on Swiss ADMET results of the synthesized compounds L₁-L₅.

com- pounds	H-bond acceptors	H-bond donors	log P _{o/w}	log S	BBB	GI absorption	Lipinski	Bioavail ability Score	TPSA	Ghose, Veber, Egan Muegge	Class
$\overline{L_1}$	4	0	3.30	-3.94	Yes	High	Yes	0.55	75.61	Yes	Soluble
L_2	4	0	3.02	-3.80	Yes	High	Yes	0.55	66.38	Yes	Moderately soluble
L_3	4	0	3.02	-3.78	Yes	High	Yes	0.55	66.38	Yes	Moderately soluble
L_4	3	0	3.77	-4.48	Yes	High	Yes	0.55	66.38	Yes	Moderately soluble
L_5	3	0	2.94	-4.88	Yes	High	Yes	0.55	66.38	Yes	Poorly soluble

flammatory drugs with minimum ulcerogenic properties. All compounds based on Veber's rules and Egan's rules represented the oral bioavailability of a possible drug molecule. Furthermore, $\log P_{\rm o/w}$ values of less than five with good lipophilicity value, indicate strong cell membrane permeability of the compounds and their biological activity. The compounds did not exhibit as CYP2D6 inhibitors, concluding that they would not show any adverse drug reactions. TPSA of compounds were measured to be less than 160 Å, demonstrating very helpful statistic for forecasting the transport of drug molecules. The drug-likeness parameters of an orally available bioactive drug are provided by the bioavailability radar and its graphical snapshot as a pink hexagonal part indicating size, flexibil-

ity, unsaturation, lipophilicity, solubility, and polarity as shown in Figure 10.

4. Conclusion

The series of five synthesized compounds L_1-L_5 in this study were prepared, purified in quantitative yield and characterized using FTIR, UV-Visible, ¹H NMR, ESI-MS and single crystal XRD. The azomethine group (-C=N-) was indicated in FTIR in the range of 1622–1690 cm⁻¹. The UV-Visible spectra showed distinct absorption band at 350 nm as an evidence of $n \rightarrow \pi^*$ transitions of azomethine group. The ¹H NMR spectra of the

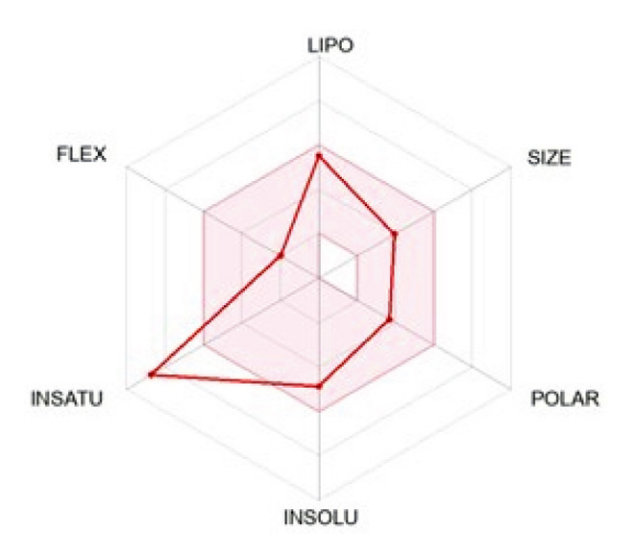


Figure 10. The bioavailability radar of the compounds L_1 – L_5 using Swiss ADME web tool.

compounds were recorded in CDCl₃ showing a peak in the range of 8.82-10.18 indicating the presence of azomethine group. All compounds demonstrated significant bioactivity against various target microbes. The antibacterial activity of all compounds were examined against Gram-negative (E. coli, K. pneumoniae and P. aeruginosa) and Gram-positive (S. aureus and S. pyogenes) bacterial strains. The activities of compounds L1-L5 against various antibacterial targets showed that compounds containing a methoxy group exhibited better activity compared to those with halogenated groups. The antioxidant activity of compounds L₁-L₅ was found to be in the order of $L_1 > L_2 > L_3 > L_5 > L_4$. The anti-fungal screening studies exhibited that all the compounds were active against C. albicans ATCC 60193 and C. tropicalis ATCC 13803 with stronger inhibitory properties compared to standard drugs. Interestingly methoxy-substituted compounds showed better bioactivities compared to halogen-substituted compounds. All compounds were optimized by DFT-D and then their quantum chemical parameters were investigated by using energy difference between the HOMO and LUMO orbitals. The chemical parameters, including energy gap and electrophilicity, obtained from DFT-D calculations, provided supportive insights into the biological activity of the compounds L_1-L_5 .

Molecular docking study exhibited good interaction in the binding pocket of *E. coli* (PDB code 4DUH) and *S. pneumoniae* (PDB code 4MOT). Finally, Swiss ADME prediction modeling evaluated the physicochemical characteristics such as solubility, permeability, and drug-likeness. Results obtained from ADME study showed GI absorption for all compounds. Observation revealed that every anticipated derivative had favorable gastric absorption, signifying noteworthy oral bioavailability. All compounds showed a wide range of lipophilicity, suggesting diverse cellular permeability and dissolution properties.

Appendix A. Supplementary data

CCDC 2455335 corresponds to the crystallographic data of compound L_1 , deposited with the Cambridge Crystallographic Data Centre. Copies of the data may be obtained free of charge from The Director, CCDC, 12, Union Road Cambridge CB21EZ [Fax: +44 (1223)336 033] or e.mail: deposit@ccdc.cam.ac.uk.

Author's Contribution

Iram Akbar and Amir Karim: Synthesis, Conceptualization, Methodology, Formal analysis, Investigation, Writing original-draft. Rahime Eshaghi Malekshah: Computational study, Biological activities, Investigation and Writing original-draft. Najeeb Ullah: Writing original-draft, Characterizations. Yu-Ting Chu and Muhammad Nawaz Tahir: X-ray Crystallography. Muhammad Iqbal: Supervision, Data curation, Formal analysis, and editing. Saqib Ali: Project administrator, Data curation, Formal analysis. Sodio C. N. Hsu: Supervision, Data curation, Formal analysis, and editing.

Acknowledgments

We thank Bacha Khan University Charsadda and Quaid I Azam University Islamabad for supporting this work. We also acknowledge Mr. Qi-Xin Guo from Department of Medicinal and Applied Chemistry of KMU for the help on the ESI-MS determination.

Declaration of Interest

The authors declare that they have no known competing financial interests or personal relationships that could have appeared to influence the work reported in this paper.

5. References

- 1. J. K. Malik, F. Manvi, B. Nanjwade, S. Singh, P. Purohit, *Pharm. Lett.* **2010**, *2*, 347–359.
- L. V. Zhilitskaya, B. A. Shainyan, N. O. Yarosh, *Molecules* 2021, 26, 2190. DOI:10.3390/molecules26082190
- 3. G. N. Raju, S. Karishma, K. R. Sowjanya, N. R. Rao, *Int. J. Adv. Pharm.* **2015**, *6*, 2776–2783.
- O. M. Salih, M. A. Al-Sha'er, H. A. Basheer, ACS Omega 2024, 9, 13928–13950. DOI:10.1021/acsomega.3c09212
- M. Singh, S. Kumar Singh, B. Thakur, P. Ray, S. K Singh, Anticancer Agents Med. Chem. 2016, 16, 722–739.
 DOI:10.2174/1871520615666151007160115
- S. Shafi, M. M. Alam, N. Mulakayala, C. Mulakayala, G. Vanaja, A. M. Kalle, R. Pallu, M. Alam, *Eur. J. Med. Chem*, 2012, 49, 324–333. DOI:10.1016/j.ejmech.2012.01.032
- 7. G. A. Pereira, A. C. Massabni, E. E. Castellano, L. A. S. Cos-

- ta, C. Q. F. Leite, F. R. Pavan, A. Cuin, *Polyhedron*, **2012**, *38*, 291–296. **DOI**:10.1016/j.poly.2012.03.016
- 8. A. Abdelhameed, X. Liao, C. A. McElroy, A. C. Joice, L. Rakotondraibe, J. Li, C. Slebodnick, P. Guo, W. D. Wilson, K. A. Werbovetz, *Bioorg. Med. Chem. Lett.* **2020**, *30*, 126725. doi: 10.1016/j.bmcl.2019.126725.
- 9. M. Gollapalli, M. Taha, M. T. Javid, N. B. Almandil, F. Rahim, A. Wadood, A. Mosaddik, M. Ibrahim, M. A. Alqahtani, Y. A. Bamarouf, *Bioorg. Chem.* **2019**, *85*, 33–48. **DOI**:10.1016/j.bioorg.2018.12.021
- M. Amir, S. Asif, I. Ali, M. Z. Hassan, Med. Chem. Res. 2012, 21, 2661–2670. DOI:10.1007/s00044-011-9791-1
- E. Kashiyama, I. Hutchinson, M.-S. Chua, S. F. Stinson, L. R. Phillips, G. Kaur, E. A. Sausville, T. D. Bradshaw, A. D. Westwell, M. F. Stevens, *J. Med. Chem.* 1999, 42, 4172–4184.
 DOI:10.1021/jm9901040
- N. Karalı, Ö. Güzel, N. Özsoy, S. Özbey, A. Salman, *Eur. J. Med. Chem.* 2010, *3*, 1068–1077.
 DOI:10.1016/j.ejmech.2009.12.001
- F. Arjmand, B. Mohani, S. Ahmad, Eur. J. Med. Chem. 2005, 40, 1103–1110. DOI:10.1016/j.ejmech.2005.05.005
- F. Arjmand, F. Sayeed, S. Parveen, S. Tabassum, A. S. Juvekar,
 M. Zingde, *Dalton Trans.* 2013, 42, 3390–3401.
 DOI:10.1039/C2DT32155F
- J. Haribabu, V. Garisetti, R. E. Malekshah, S. Srividya, D. Gayathri, N. Bhuvanesh, R. V. Mangalaraja, C. Echeverria, R. Karvembu, *J. Mol. Struct.* 2022, 1250, 131782.
 DOI:10.1016/j.molstruc.2021.131782
- J. K. Suyambulingam, R. Karvembu, N. S. Bhuvanesh, I. V. M. V. Enoch, P. M. Selvakumar, D. Premnath, C. Subramanian, P. Mayakrishnan, S.-H. Kim, I.-M. Chung, J. Adhes. Sci. Technol. 2020, 34, 2590–2612. DOI:10.1080/01694243.2020.1775032
- 17. M. Vedavathi, B. Somashekar, G. Sreenivasa, E. Jayachandran, *Int. J. Pharm. Sci. Res.* **2010**, 2, 53.
- S. Salman, N. Bakr, M. Mahmood, *Physics and Astronomy*, ILCPA. 2015, 40, 36–42. DOI:10.56431/p-q9tzpl
- 19. N. D. Amnerkar, B. A. Bhongade, K. P. Bhusari, *Arab. J. Chem.* **2015**, *8*, 545–552. **DOI:**10.1016/j.arabjc.2014.11.034
- A. Rambabu, M. P. Kumar, S. Tejaswi, N. Vamsikrishna, *J. Photochem. Photobiol. B.* 2016, *165*, 147–156.
 DOI:10.1016/j.jphotobiol.2016.10.027
- 21. M. N. Bhoi, M. A. Borad, H. D. Patel, Synth. Commun. 2014, 44, 2427–2457. DOI:10.1080/00397911.2014.907426
- H. S. Lihumis, A. A. Alameri, R. H. Zaooli, *Prog. Chem. Biochem. Res.* 2022, 5, 147–164.
 DOI:10.22034/pcbr.2022.330703.1214
- 23. L. Lerman, *J. Mol. Biol.* **1961**, *3*, 18–14. **DOI:** 10.22034/pcbr.2022.330703.1214
- S. Dayan, M. Tercan, F. A. Özdemir, G. Aykutoğlu, N. Özdemir, Z. Şerbetçi, M. Dinçer, O. Dayan, *Polyhedron*, 2021, 199, 115106. DOI:10.1016/j.poly.2021.115106
- S. Upadhyay, R. Zala, K. Bhatt, Med. Anal. Chem. Int. J. 2020, 4, 1–7. DOI:10.23880/macij-16000157
- M. T. Gabr, N. S. El-Gohary, E. R. El-Bendary, M. M. El-Kerdawy, N. Ni, *Chin. Chem. Lett.* 2016, 27, 380–386.
 DOI:10.1016/j.cclet.2015.12.033

- Y. Belay, A. Muller, P. Leballo, O. A. Kolawole, A. S. Adeyinka,
 T. Y. Fonkui, L. R. Motadi, *J. Mol. Struct.* 2023, 1286, 135617.
 DOI:10.1016/j.molstruc.2023.135617
- K. Gholivand, M. Sabaghian, R. E. Malekshah, *Bioorg. Chem.* 2021, 115, 105193. DOI:10.1016/j.bioorg.2021.105193
- R. Eshaghi Malekshah, M. Salehi, M. Kubicki, A. Khaleghian, J. Coord. Chem. 2018, 71, 952–968.
 DOI:10.1080/00958972.2018.1447668
- A. L. Spek, Biol. Crystallogr. 2009, 65, 148–155.
 DOI:10.1107/S090744490804362X
- J. Lübben, C. M. Wandtke, C. B. Hübschle, M. Ruf, G. M. Sheldrick, B. Dittrich, *Found. Crystallogr.* 2019, 75, 50–62.
 DOI:10.1107/S2053273318013840
- A. Abdelmadjid, D. Haffar, F. Benghanem, S. Ghedjati, L. Toukal, V. Dorcet, R. Bourzami, *J. Mol. Struct.* 2021, 1227, 129368. DOI:10.1016/j.molstruc.2020.129368
- H. Ighnih, R. Haounati, R. E. Malekshah, H. Ouachtak, Y. Toubi, F. Alakhras, A. Jada, A. A. Addi, *JPPA*, 2023, 445, 115071. DOI:10.1016/j.jphotochem.2023.115071
- 34. M. Haghbin, R. Eshaghi Malekshah, M. Sobhani, Z. Izadi, B. Haghshenas, M. Ghasemi, B. S. Kalani, H. Samadian, *Int. J. Biol. Macromol.* **2023**, *235*, 123766. **DOI:**10.1016/j.ijbiomac.2023.123766
- S. Parvarinezhad, M. Salehi, R. Eshaghi Malekshah, M. Kubicki, A. Khaleghian, *Appl. Organomet. Chem.* 2022, 36, e6563. DOI:10.1002/aoc.6563
- G. Alpaslan, B. Boyacioglu, N. Demir, Y. Tümer, G. Yapar,
 N. Yıldırım, M. Yıldız, H. Ünver, J. Mol. Struct. 2019, 1180,
 170–178. DOI:10.1016/j.molstruc.2018.11.065
- E. Ogbonda-Chukwu, O. Abayeh, O. Achugasim, *J. Appl. Sci. Environ. Manage.* 2022, 26, 2033–2037.
 DOI:10.4314/jasem.v26i12.17
- 38. E.-A. D. M. Abd, E. S. Eldin H, Ali Elham A. *J. Mol. Struct.* **2013**, *1048*, 487–499. **DOI:**10.1016/j.molstruc.2013.05.051
- 39. S. Noreen, S. H. Sumrra, *ACS Omega*, **2021**, *6*, 33085–33099. **DOI:**10.1021/acsomega.1c05290
- M. Sunjuk, L. Al-Najjar, M. Shtaiwi, B. El-Eswed, M. Al-Noaimi, L. Al-Essa, K. Sweidan, *Inorganics*, 2022, 10, 43.
 DOI:10.3390/inorganics10040043
- S. Chacko, S. Samanta, *J. Biopha.* 2017, 89, 162–176.
 DOI:10.1016/j.biopha.2017.01.108
- 42. A. Ahlawat, V. Singh, S. Asija, *Chem. Pap.* **2017**, *71*, 2195–2208. **DOI**:10.1007/s11696-017-0213-9
- 43. Y. S. Demircioğlu, H. C. Sakarya, Y. Süzen, *Bulg. Chem. Commun.* **2020**, *52*, 9–13. **DOI:** 10.34049/bcc.52.1.4835
- O. A. El-Gammal, A. A. El-Bindary, F. S. Mohamed, G. N. Rezk, M. A. *J. Mol. Liq.* 2022, 34, xx–xx.
 DOI:10.1016/j.molliq.2021.117850
- F. Lemilemu, M. Bitew, T. B. Demissie, R. Eswaramoorthy, M. Endale, *BMC Chemistry*, 2021, 15, 67.
 DOI:10.1186/s13065-021-00791-w
- N. Ranjitha, G. Krishnamurthy, M. Manjunatha, H. B. Naik, M. Pari, N. Vasantakumarnaik, J. Lakshmikantha, K. Pradeepa, *J. Mol. Struct.* 2023, 1274, 134483.
 DOI:10.1016/j.molstruc.2022.134483
- 47. H. A. K. Kyhoiesh, K. J. Al-Adilee, Inorganica Chim. Acta.

- **2023**, 555, 121598. **DOI:**10.1016/j.ica.2023.121598
- 48. Y. Cai, Q. Luo, M. Sun, H. Corke, *Life Sci.* **2004**, *74*, 2157–2184. **DOI**:10.1016/j.lfs.2003.09.047
- A. C. Ekennia, A. A. Osowole, L. O. Olasunkanmi, D. C. Onwudiwe, E. E. Ebenso, *Res. Chem. Intermed.* 2017, 43, 3787–3811. DOI:10.1007/s11164-016-2841-z
- S. Sakthivel, T. Alagesan, S. Muthu, C. S. Abraham, E. Geetha, J. Mol. Struct. 2018, 1156, 645–656.
 DOI:10.1016/j.molstruc.2017.12.024
- 51. R. Gandhimathi, S. Anbuselvi, R. Saranya, *JICS* **2023**, *100*, 101033. **DOI**:10.1016/j.jics.2023.101033
- 52. B. Belhani, M. Aissaoui, H. K'tir, T. Khaldi, L. Khattabi, Y. La-

- ichi, A. Boulebnane, M. Berredjem, S. E. Djilani, *J. Mol. Struct.* **2023**, *1293*, 136221. **DOI:**10.1016/j.molstruc.2023.136221
- A. Bayazeed, H. Alharbi, A. I. Alalawy, N. A. H. Alshammari, A. M. Alqahtani, M. Alsahag, A. Alisaac, N. M. El-Metwaly, *J. Mol. Struct.* 2025, *1320*, 139579.
 DOI:10.1016/j.molstruc.2024.139579
- W. M. Alamoudi, J. Saudi Chem. Soc. 2024, 28, 101897.
 DOI:10.1016/j.jscs.2024.101897
- A. Bhardwaj, M. Kumar, S. Garg, D. Kumar, *Inorg. Chem. Commun.* 2023, 157, 111332. DOI:10.1016/j.inoche.2023.111332
- S. Banwala, S. Sardana, R. K. Sindhu, REDVET 2024, 25, 584–599. DOI:10.53555/redvet.v25i1.601

Povzetek

V tej študiji smo sintetizirali serijo novih kondenzacijskih produktov L_1 – L_5 , ki so nastali med substituiranimi piridinkarbaldehidi in 2-aminobenzotiazolom. Spojine smo karakterizirali s FTIR, UV-Vis, ¹H NMR spektroskopijo in ESI-MS analizami. Dodatno smo spojino L_1 strukturno določili s pomočjo rentgenske difrakcije monokristala; ugotovili smo, da v asimetrični enoti vsebuje štiri kristalografsko neodvisne molekule. Vse pripravljene spojine izkazujejo antibakterijsko aktivnost proti Gram-negativnim in Gram-pozitivnim bakterijam ter so aktivne tudi proti *Candida albicans* ATCC 60193 in *Candida tropicalis* ATCC 13803. Strukture vseh spojin smo optimizirali s DFT-D metodo nato pa zanje izračunali vrednosti celokupnih energij ter vrednosti HOMO in LUMO energij ter določili teoretične parametre reaktivnosti. Napovedane ADME lastnosti nakazujejo, da vse spojine izkazujejo dobro podobnost z zdravili in da imajo ustrezne farmakokinetične lastnosti.



Except when otherwise noted, articles in this journal are published under the terms and conditions of the Creative Commons Attribution 4.0 International License